Blackbody-Like Infrared Radiation in Stacked Graphene P–N Junction Diode

N. Murakami*, Y. Sugiyama, Y. Ohno, M. Nagase

Graduate School of Advanced Technology and Science, Tokushima University, Minamijyosanjima 2–1, Tokushima 770–8506, Japan

*E-mail: n_murakami@ee.tokushima-u.ac.jp; nagase@ee.tokushima-u.ac.jp

Abstract

The electrical and optical properties of a stacked graphene p–n junction were investigated. N-type and p-type graphene films epitaxially grown on a SiC substrate were directly bonded to each other in a face-to-face manner. The current–voltage characteristics of the graphene junction diode exhibited an Ohmic behavior below 20 V. The conductance increased in the bias range above 20 V and had a peak around 65 V. The emission spectrum and temperature of the graphene p–n junction were measured using Fourier-transform far-infrared (FTIR) spectroscopy and infrared bolometer array. An electrically induced blackbody-like radiation with a peak wavelength of 10.2 μm was observed. Although the temperature change estimated using the bolometer results was 66 K at a power of 1.2 W, the peak wavelength of the FTIR spectrum was constant. An electrically induced blackbody-like far-infrared emission diode with a defined peak wavelength was successfully realized using the stacked graphene p–n junctions.

1. Introduction

Graphene, a two-dimensional (2D) material, has attracted considerable attention because of its singular electronic physical properties[1,2] originating from the linear dispersion relation with zero bandgap. Extensive experimental and theoretical studies have been carried out on graphene for functional devices including photoemitters[3–6], photodetectors[7], optical modulators[8], plasmonic devices[9–11], and tunnel junction devices[3,12–14]. Particularly, optical devices operating with infrared to terahertz (THz) waves have been increasingly investigated for various applications of imaging[15], wireless communications[16], and spectroscopy[17,18]. However, the lack of devices that can emit infrared to THz waves with high outputs and small sizes at room temperature hinders further applications. Therefore, this study focuses on fabrication of optical devices that can emit high-power infrared-to-THz waves.

In this paper, we report the electrical and optical properties of a junction diode device consisting of a single-crystal monolayer n-doped graphene and p-doped graphene stacked in a face-to-face manner. The measured *I–V* characteristics of the vertically stacked graphene junction diode exhibited nonlinear behaviors in the highly biased regime, despite the Ohmic characteristics in the reported lateral p–n junctions[19,20]. Owing to the large device size (100 mm^2), the stacked graphene diode could be applied over 1 W. The Joule heating effect should heat the junction. A temperature measurement using a thermo-camera with a bolometer and infrared spectrum measurement using a Fourier-transform infrared (FTIR) spectrometer were performed. The efficiency of the infrared emission was estimated using the temperature change measured by an infrared bolometer. A blackbody-like emission spectrum with a constant peak wavelength was observed in the FTIR spectrum. These results can pave the way for the realization of optical devices with graphene and broaden the applications for various technologies.

2. Experimental methods

2.1 Fabrication of epitaxial graphene samples

The graphene samples were epitaxially grown using an infrared rapid thermal annealer (Thermo Riko SR-1800)[21]. The initial substrate was a semi-insulating 4H-SiC (0001)

substrate (100 mm^2). For sample A, the SiC substrate was annealed at 1700 °C in an Ar environment (100 Torr) for 1 s to prepare a buffer layer of one-monolayer carbon. For sample B, the annealing was carried out at 1580 °C in an Ar environment (100 Torr) for 5 min to prepare a monolayer graphene with a buffer layer. The layer number and quality of graphene were confirmed using microscopic Raman spectroscopy (Technospec uRaman532). Sample A was electrically insulative in the as-grown state. The growth of the buffer layer ($6\sqrt{3} \times 6\sqrt{3}$ structure) was confirmed by Raman spectroscopy. The as-grown graphene on 4H-SiC (0001) was n-doped because of the interactions with the substrates such as the buffer layers, carrier scattering, and dangling bonds. Regarding the n-type graphene, sample B had a sheet resistance of 2400 Ω/□, carrier mobility of 1500 $cm^2\ V^{-1}\ s^{-1}$, and sheet carrier (electron) density of $1.7 \times 10^{12}\ cm^{-2}$. Raman mapping results indicate that sample B was covered with a monolayer graphene film considering the full width at half maximum of the 2D band peak of 36 cm^{-1} [22].

2.2 Fabrication of p-doped graphene with the hydrogen intercalation technique

We performed hydrogen intercalation[23–25] to change the carrier type of graphene from n-type to p-type. Sample A was annealed in Ar+H_2 at 1000 °C for 60 min. After the hydrogen annealing, the carrier type of sample A was p-type. A Hall effect measurement showed that sample B had a sheet resistance of 1000 Ω/□, carrier mobility of 700 $cm^2\ V^{-1}\ s^{-1}$, and sheet carrier (hole) density of $8.6 \times 10^{12}\ cm^{-2}$. We observed a 2D peak (35 cm^{-1}), which showed the presence of monolayer graphene on SiC through a microscopic Raman analysis after the hydrogen intercalation, and decrease in the buffer layer signal.

2.3 Fabrication of the stacked graphene p–n junction

Sample A, p-type quasi-free-standing monolayer graphene, and sample B, n-type as-grown monolayer graphene on a SiC substrate, were directly bonded to each other in a face-to-face manner, as shown in Fig. 1. The two samples were twisted to an azimuth angle of 60° for crystallographic alignment of the substrates. The samples were fixed with acrylic molds. Four gold-coated contact probes were placed on the sample surface for Ohmic contacts.

3. Results and discussion

3.1 Electrical characteristics of the stacked p–n junction

Figure 2 shows the electrical characteristics of the stacked graphene p–n junction measured using a semiconductor device analyzer (Keysight Technologies B1500A). Figure 2(a) shows the *I–V* characteristics obtained by the four-terminal and two-terminal methods. Both measurements showed strictly linear characteristics, which indicates that the graphene p–n junction and graphene–metal junction were Ohmic. The two-terminal and four-terminal resistances were 6.9 and 0.8 kΩ, respectively. Linear *I–V* characteristics in gate-controlled p–n junctions that create p-doped and n-doped regions on the same surface[23] and lateral p–n junction created by electron-beam irradiation[24] have been observed. The linear characteristic at a low bias voltage is attributed to the absence of bandgap of graphene and linear dispersion relation described by a Dirac cone.

Figure 3 shows the (a) *I–V* characteristic and (b) d*I*/d*V* plot up to 80 V measured in the two-terminal regime. Figure 3(b) shows almost constant values up to 20 V, which increase above 20 V, exhibiting nonlinearity, different from the behavior of the previous lateral p–n junction. The differential conductance rapidly increased and reached a value approximately 8 times the initial value at 65 V. The junction voltage was estimated to be 5 V at the diode bias of 65 V. In the high-bias regime, the density of states for graphene does not exhibit the linear dispersion. A previous study demonstrated that the density of states for graphene exhibited a semimetallic behavior far from the Dirac point; both electron and hole densities of states had a steep peak at the van Hove singularity[26]. More detailed experiments are required to elucidate the relationship between the *I–V* characteristic shown in Fig. 3(b) and density of states for graphene.

3.2 Thermal measurement with the bolometer

Temperature measurements were performed using a thermal imaging camera (FLIR ETS320). Figure 4(a) shows an infrared image in the junction region at 40 V. The region surrounded by the black rectangle is a device part of stacked graphene on the SiC substrate, as shown in the schematic in Fig. 2(a). At this bias, the temperature of the junction area increased to 42 °C. The power dependence of the temperature change is shown in Fig. 4(b). The temperature change linearly increases with the applied power. The bolometer of the

thermal imaging camera measures the infrared radiation intensity, which can be converted to the temperature if the radiation from the sample is blackbody radiation. The results in Fig. 4(b) indicate that the electrical power is directly converted to infrared radiation power.

The conversion efficiency α of electrical power to infrared radiation power can be estimated using the Stefan–Boltzmann's law. We defined the efficiency α by

$$E = \frac{\alpha P}{S} = \sigma T^4, \quad (1)$$

where T is the temperature (K) of blackbody radiation, E is the energy density (W/m^2), σ is the Stefan–Boltzmann constant, S is the radiation area, and P is the applied electrical power (W),

$$P = R_{2T} I^2, \quad (2)$$

where R_{2T} is the two-terminal resistance of the stacked graphene diode. The temperature change ΔT can be expressed by

$$\Delta T = \sqrt[4]{\frac{P\alpha}{\sigma S} + T_0^4} - T_0, \quad (3)$$

where T_0 is the initial temperature. By fitting Eq. (3) to the measured temperature change shown in Fig. 4(b), the radiation efficiency α was estimated to be 10%. This efficiency is very high compared to that of the reported graphene blackbody emitter[6].

3.3 Optical characteristics of the stacked p–n junction

Infrared spectral measurements were performed using an FTIR instrument (JASCO FT/IR-6600) at room temperature under atmospheric pressure. The stacked graphene diode was biased using voltage/current source meters (Keithley 2450). The measured radiation

spectrum of the stacked graphene p–n junction is shown in Fig. 5(a). The radiation spectrum at 0 V was subtracted from the background. The peak wavelength of the measured infrared spectrum was almost constant, 10.2 μm, which corresponds to a blackbody temperature of 284 K estimated by the Planck's law. The dotted line in Fig. 5(a) is a calculated spectrum of a 284-K blackbody. As the FTIR spectroscopy measurements were performed in air, absorption fingerprints were observed in the spectrum. The intensity reductions around 7 and 20–30 μm are attributed to H_2O. The reduction around 15 μm is attributed to CO_2 absorption. The small dip at approximately 12 μm is attributed to the effect of the SiC substrate[27]. Figure 5(b) shows the electrical power dependence of the total emission intensity measured by FTIR spectroscopy. The total emission intensity increased almost linearly with the applied power. This corresponds with the results of the thermal camera measurement shown in Fig. 4(b) because the bolometer measures the infrared emission power. Surprisingly, the peak wavelengths of the measured FTIR spectra were almost constant when the applied electrical power increased, as shown in Fig. 6. The peak wavelengths estimated using the junction temperature measured by the thermal camera are also shown in Fig. 6. If the emission spectrum in Fig. 5(a) corresponds to blackbody emission caused by Joule heating, the peak wavelength at 1.3 W (80 V) should shift to approximately 8 μm. However, the peak wavelength of the measured spectrum at 80 V was 10.2 μm. This suggests that these blackbody-like emission spectra are attributed to a nonthermal emission mechanism. A light wavelength of 10.2 μm corresponds to a photon energy of 122 meV. The Fuchs–Kliewer (F–K) surface phonon energy of SiC (0001) is 117 meV, close to the measured value[28,29]. The blackbody-like emission from the stacked epitaxial graphene junction may be attributed to the F–K phonon emission electrically induced by carriers in graphene. Interactions between sheet plasmons in graphene and substrate phonons have been discussed for graphene on SiO_2[30], h-BN[31], and SiC[32,33] substrates. The graphene electric states were modified by the substrate phonons owing to the plasmon–phonon coupling described through surface phonon plasmon polaritons[30,31]. An unusually strong coupling between 2D optical plasmons in monolayer or multilayer graphene and F–K phonon of the SiC substrate was observed by angle-resolved reflection electron energy loss spectroscopy[32] and high-resolution electron energy loss spectroscopy[33].

A blackbody-like infrared emission diode with a constant peak wavelength was

successfully demonstrated using the vertically stacked graphene p–n junction. The mechanisms responsible for the nonlinear *I–V* characteristics and blackbody-like far-infrared emission are unclear, and thus further investigation is required to understand them. The high conversion efficiency of the stacked graphene diode is promising. If a graphene acoustic phonon[34,35] whose energy is lower than those of graphene optical phonons and F–K phonons of SiC can be electrically induced, a THz emission diode will be realized.

4. Conclusions

We fabricated a stacked graphene ṕ–n junction comprising two epitaxial graphene layers on SiC substrates. In the electrical measurement, the *I–V* characteristic of the stacked graphene p–n junction exhibited nonlinearity because the graphene density of states in the high-energy regime appeared owing to the strong electric field. The electrically induced blackbody-like radiation without temperature increase in the stacked graphene p–n junction diode was observed by FTIR spectroscopy. The measured radiation intensity almost linearly increased with the applied electric power, whereas the peak wavelength of the emission spectrum was constant, 10.2 μm. The conversion efficiency of the far-infrared emission estimated using the bolometer was 10%. The results suggest that this intriguing radiation mechanism is attributed to the F–K phonon of graphene on SiC (0001).

ACKNOWLEDGMENT

This study was partly supported by KAKENHI Grant Number JP19H02582 and the Cooperative Research Project Program of the Research Institute of Communication, Tohoku University.

References

1) K. S. Novoselov, A. K. Geim, S. V. Morozov, D. Jiang, Y. Zhang, S. V. Dubonos, I. V. Grigorieva, and A. A. Firsov, Science **306**, 666 (2004).
2) K. S. Novoselov, A. K. Geim, S. V. Morozov, D. Jiang, M. I. Katsnelson, I. V. Grigorieva, S. V. Dubonos, and A. A. Firsov, Nature **438**, 197 (2005).
3) V. Ryzhii, A. A. Dubinov, V. Y. Aleshkin, M. Ryzhii, and T. Otsuji, Appl. Phys. Lett. **103**, 163507 (2013).
4) D. Yadav, S. B. Tombet, T. Watanabe, S. Arnold, V. Ryzhii and T. Otsuji, 2D Materials **3**, 045009 (2016).
5) A. A. Dubinov, V. Y Aleshkin, M. Ryzhii, T. Otsuji, and V. Ryzhii, Appl. Phys. Express **2**, 092301 (2009).
6) Y. D. Kim, Y. Gao, R. Shiue, L. Wang, O. B. Aslan, M. Bae, H. Kim, D. Seo, H. Choi, S. H. Kim, A. Nemilentsau, T. Low, C. Tan, D. K. Efetov, T. Taniguchi, K. Watanabe, K. L. Shepard, T. F. Heinz, D. Englund, and J. Hone, Nano Lett. **18**, 934 (2018).
7) F. Xia, T. Mueller, Y. Lin, A. Valdes-Garcia and P. Avouris, Nature Nanotechnology **4**, 839 (2009).
8) M. Liu, X. Yin, E. Ulin-Avila, B. Geng, T. Zentgraf, L. Ju, F. Wang and Xiang Zhang, Nature **474**, 64 (2011).
9) T.J. Echtermeyer, L. Britnell, P.K. Jasnos, A. Lombardo, R.V. Gorbachev, A.n. Grigorenko, A.K. Geim, A.C. Ferrari and K.s. novoselov, Nature Communications **2**, 458 (2011).
10) T. Low and P. Avouris, ACS Nano **8**, 1086 (2014).
11) Q. Deng, H. Shao, W. He, K. Cheng, J. Hu, B. Sun, X. Wang, G. Liu and J. Wang, Plasmonics **14**, 993 (2019).
12) L. Britnell, R. V. Gorbachev, A. K. Geim, L. A. Ponomarenko, A. Mishchenko, M. T. Greenaway, T. M. Fromhold, K. S. Novoselov, and L. Eaves, Nat. Commun. **4**, 1794 (2013).
13) A. Woessner, A. Misra, Y. Cao, I. Torre, A. Mishchenko, M. B. Lundeberg, K. Watanabe, T. Taniguchi, M. Polini, K. S. Novoselov, and F. H. L. Koppens, ACS Photonics **4**, 3012 (2017).
14) J. Du, Y. Kimura, M. Tahara, K. Matsui, H. Teratani, Y. Ohno, and M. Nagase, Jpn. J. Appl. Phys. **58**, SDDE01 (2019).
15) K. Kawase, Y. Ogawa, Y. Watanabe, Optics Express **11**, 2549 (2003).
16) T. Kleine-Ostmann and T. Nagatsuma, Journal of Infrared, Millimeter, and Terahertz Waves **32**, 143 (2011).
17) M. C. Beard, G. M. Turner, and C. A. Schmuttenmae, J. Phys. Chem. B **106**, 7146 (2002).
18) A. G. Davies, A. D. Burnett, W. Fan, E. H. Linfield and J. E. Cunningham, materialstoday **11**, 18 (2008).
19) J. R. Williams, L. DiCarlo, C. M. Marcus, Science. **317** (5838), 638 (2007).
20) X. Yu, Y. Shen, T. Liu, T. Wu and Q. J. Wang, Scientific Reports 5, 12014 (2015).
21) T. Aritsuki, T. Nakashima, K. Kobayashi, Y. Ohno, and M. Nagase, Jpn. J. Appl. Phys. **55**, 06GF03 (2016).
22) R. O, A. Iwamoto, Y. Nishi, Y. Funase, T. Yuasa, T. Tomita, M. Nagase, H. Hibino and H. Yamaguchi, Jpn. J. Appl. Phys. **51**, 06FD06 (2012).
23) S. Tanabe, M. Takamura, Y. Harada, H. Kageshima and H. Hibino, Jpn. J. Appl. Phys. **53**, 04EN01 (2014).
24) C. Riedl, C. Coletti, T. Iwasaki, A. A. Zakharov, and U. Starke, Phys. Rev. Lett. **103**, 246804 (2009).
25) J. Kunca, M. Rejhon, and P. Hlídek, AIP Advances **8**, 045015 (2018).
26) A. H. Castro Neto, F. Guinea, N. M. R. Peres, K. S. Novoselov, and A. K. Geim, Rev.,Mod. Phys. **81**, 109 (2009).
27) K. M. Pitman, A. M. Hofmeister, A. B. Corman and A. K. Speck, A&A **483**, 66 (2008).
28) H. Nienhaus, T.U. Kampen and W. Mönch, Surface Science **324**, L328 (1995).

29) J. Lu, K. P. Loh, H. Huang, W. Chen, and A. T. S. Wee, Phys. Rev. **80**, 113410 (2009).
30) V. W. Brar, M. S. Jang, M. Sherrott, J. J. Lopez, and H. A. Atwater, Nano Lett. **13** (6), 2541 (2013).
31) V. W. Brar, M. S. Jang, M. Sherrott, S. Kim, J. J. Lopez, L. B. Kim, M. Choi, and H. Atwater, Nano Lett. **14** (7), 3876 (2014).
32) Y. Liu and R. F. Willis, Phys. Rev. B **81**, 081102 (2010).
33) R. J. Koch, Th. Seyller, and J. A. Schaefer, J. A. Phys. Rev. B **82** (20), 201413 (2010).
34) E. H. Hwang and S. D. Sarma, Phys. Rev. B **77**, 115449 (2008).
35) K. Kaasbjerg, K. S. Thygesen, and K. W. Jacobsen, Phys. Rev. B **85**, 165440 (2012).

Figure Captions

Fig. 1. (a) Top schematic and (b) side schematic of the device structure of the stacked graphene p–n junction. Two samples, p-type and n-type graphene on the SiC substrate, were directly bonded to each other at an azimuth angle of 60° for crystallographic alignment. Gold coating contact probes were used for electrical connections for the graphene films. (c) Device photograph. The two samples were fixed by acrylic molds.

Fig. 2. *I–V* characteristics obtained by the four-terminal and two-terminal methods up to ±10 V. Both curves show linear relationships between the diode current and bias voltage.

Fig. 3. (a) *I–V* characteristic obtained by the two-terminal method up to 80 V. (b) Differential conductance (d*I*/d*V*) plot. The conductance of the stacked graphene diode is almost constant up to 20 V, and then gradually increases above 20 V. A sharp increase is observed above 55 V.

Fig. 4. (a) Infrared radiation image in the junction region at 40 V. The bright area surrounded by the black rectangle (12 mm × 1 mm) indicates the graphene p–n junction diode. (b) Power dependence of the temperature change.

Fig. 5. (a) Radiation spectra of the stacked graphene p–n junction measured by FTIR spectroscopy. The dotted line is a calculated blackbody radiation spectrum at 284 K. (b) Power dependence of the total emission intensity. The total intensity increased almost linearly with the applied electrical power.

Fig. 6. Peak wavelength of the blackbody-like spectrum measured by FTIR spectroscopy (Fig. 5(a)), shown by the solid circles. The averaged peak wavelength, 10.2 μm, is expressed by the solid line. The peak wavelengths estimated using the temperature results measured using the thermal camera are shown by the square symbols and dotted line.

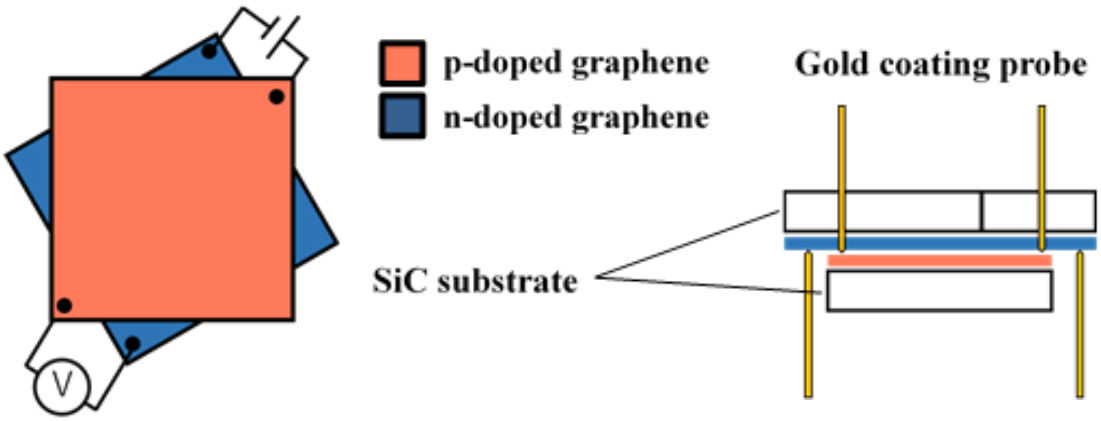
p-doped graphene
n-doped graphene
Gold coating probe
SiC substrate
V

(a) (b)

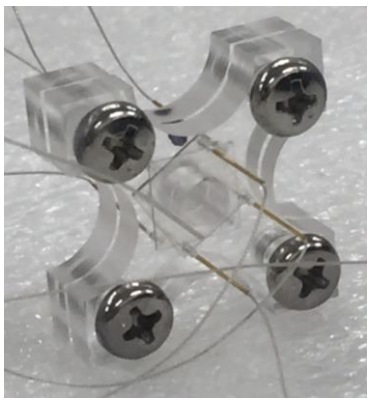

(c)

Fig.1.

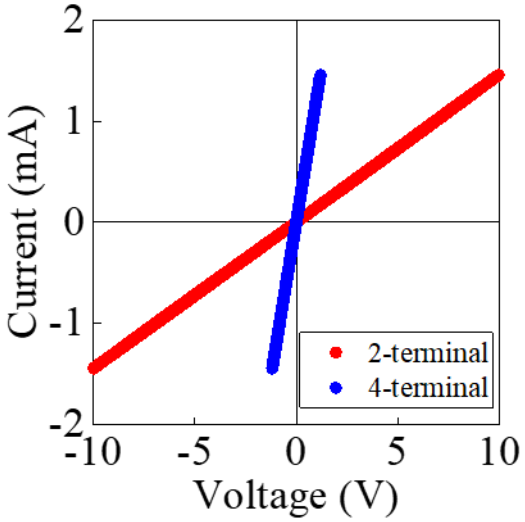
Current (mA)
Voltage (V)
2-terminal
4-terminal
2
1
0
-1
-2
-10
-5
0
5
10

Fig.2.

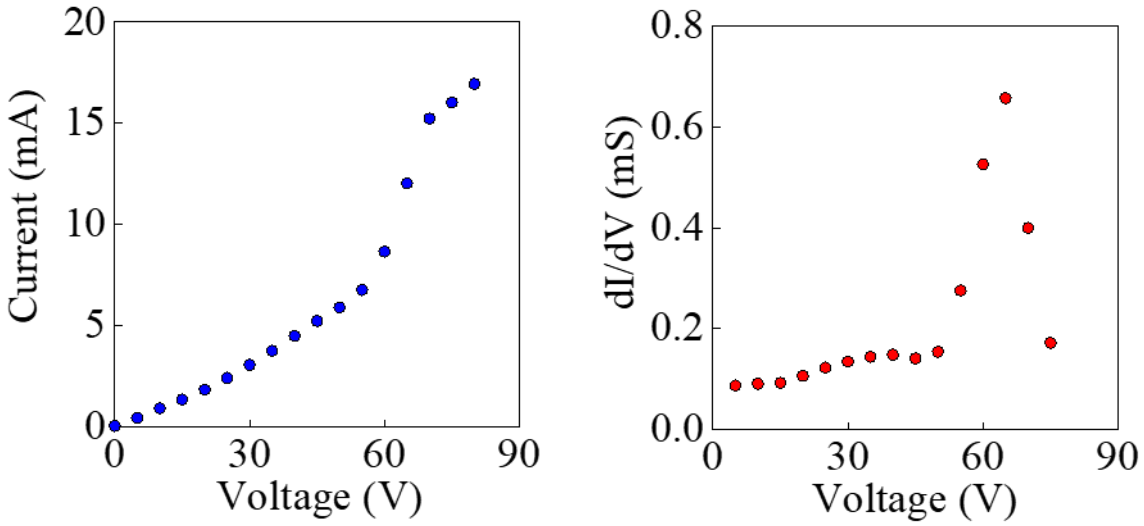
Current (mA)
Voltage (V)
dI/dV (mS)
Voltage (V)
20
15
10
5
0
0
30
60
90
0.8
0.6
0.4
0.2
0.0

(a) (b)

Fig.3.

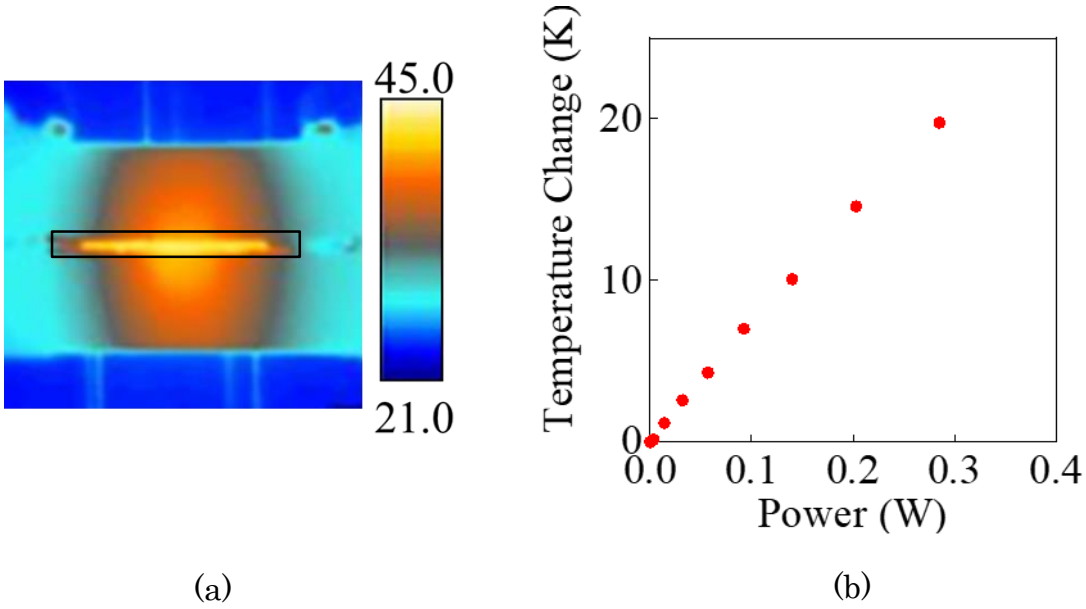

(a) (b)

Fig.4.

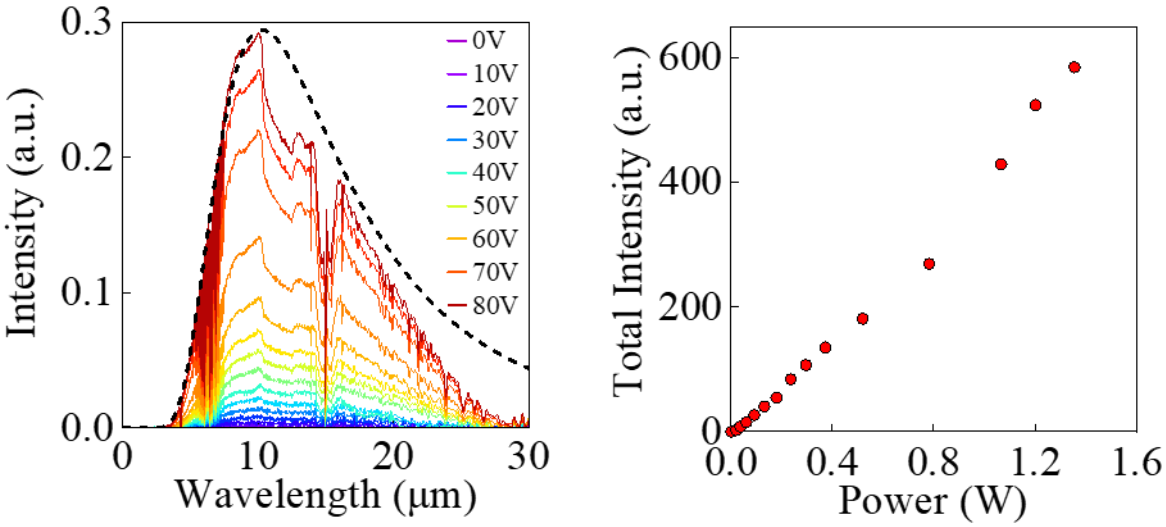

(a) (b)

Fig.5.

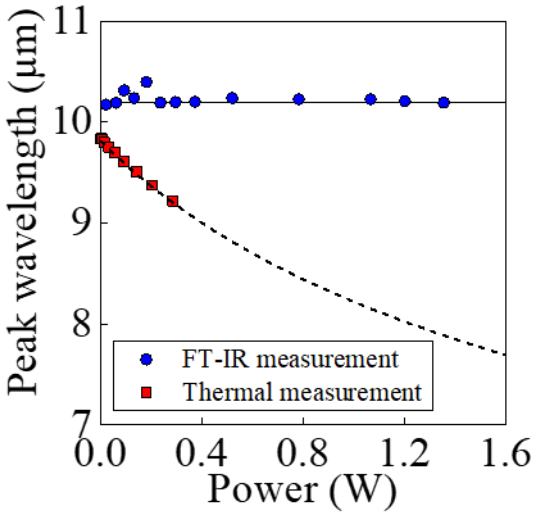
Peak wavelength (μm)
11
10
9
8
7
0.0
0.4
0.8
1.2
1.6
Power (W)
FT-IR measurement
Thermal measurement

Fig.6.